International Journal of Applied Pharmaceutics

ISSN- 0975-7058 Vol 18, Issue 1, 2026

9Original Article

DESIGN CHARACTERIZATION OPTIMIZATION OF LENALIDOMIDE-LOADED BOVINE SERUM ALBUMIN NANOPARTICLES FOR MYELOMA THERAPY

SAMEENA BEGUM[1], NIRANJAN PANDA[2], CH. PRAVEENA[3*]

[1]Department of Pharmacy, Chaitanya Deemed to be University, Warangal-506001, Telangana. [2]School of Pharmacy, the Neotia University, 24 Parganas (South), West Bengal-743368, India. [3*]Department of Pharmacy, Chaitanya Deemed to be University, Warangal-506001, Telangana, India

[*]Corresponding author: CH. Praveena; [*]Email: praveenamr18@gmail.com

Received: 16 Jun 2025, Revised and Accepted: 15 Oct 2025

ABSTRACT

Objective: The present investigation focuses on the formulation and optimization of lenalidomide (LD)-loaded bovine serum albumin (BSA) nanoparticles (NPs) using the desolvation method. Box-Behnken design (BBD) was implemented to optimize the formulation.

Methods: The desolvation technique was employed to synthesize BSA-NPs encapsulating LD and characterized by particle size analysis, zeta potential, and transmission electron microscopy (TEM) analysis.

Results: The findings confirmed that the uniform spherical NPs were formed below 200 nm. Particle size found in the range of 110.9±13.02 nm to 182.8±10.33 nm, entrapment efficiency (EE) found between 60.1±9.01% and 94.80±9.14% and zeta potential-15.3±0.21mV to-29.7 ±0.12mV. A sudden burst release of approximately 55.68% was observed within 4 h from optimized LD BSA NPs (Opt-LD-BSA-NPs), followed by a slower release over 24 h. *In vitro*, cytotoxicity assays demonstrated selective toxicity against U266 cancer cells. The Opt-LD-BSA-NPs exhibited a significantly lower half-maximal inhibitory concentration (IC50) of 29.70%, indicating enhanced cytotoxic efficacy. Fourier transform infrared spectroscopy (FTIR) and differential scanning calorimetry (DSC) analyses indicated successful drug entrapment and a transition of LD from a crystalline to an amorphous form. The area under curve (AUC) for Opt-LD-BSA-NPs was found to be 22.47 µg/ml/hr, which is 3 times more than the pure LD suspension (6.3025 µg/ml/h). It revealed enhanced bioavailability.

Conclusion: These findings underscore the potential of BSA-based nanocarriers to enhance the solubility, stability, and therapeutic efficacy of hydrophobic anticancer agents, such as LD.

Keywords: BSA, Nanoparticle, Myeloma, Optimization, Lenalidomide

DOI: https://dx.doi.org/10.22159/ijap.2026v18i1.55623 Journal homepage: https://innovareacademics.in/journals/index.php/ijap

INTRODUCTION

Cancer is a serious and often fatal disease caused by the abnormal growth and spread of cells in the body [1]. Normally, cells grow and die in a controlled way, but in cancer, this process is disrupted, leading to tumour formation and potential spread to other organs [2]. There are over 100 types of cancer, named after the affected organ or cell type, such as breast cancer and leukaemia. While the exact cause is unclear, common risk factors include smoking, alcohol, poor diet, inactivity, radiation, infections, and genetics [3]. Early detection and proper treatment-such as surgery, chemotherapy, and radiation-can greatly improve survival. Raising awareness about prevention and early diagnosis is essential in fighting cancer globally [4].

In cancer, the cell cycle of normal cells, which regulates how cells grow, divide, and die, is disrupted. Under normal circumstances, the cell cycle has checkpoints that make cells divide only when necessary and that destroy or repair damaged cells [5]. In cancer, these checkpoints are lost because of genetic mutations, which permit damaged or abnormal cells to continue dividing uncontrollably [6]. This results in tumor formation and, in certain instances, the dissemination of cancer to distant sites in the body. Central regulatory proteins such as cyclins and tumor suppressor genes (e.g., p53) tend to become defective in cancer cells and are responsible for this loss of regulation [7].

Bovine serum albumin nanoparticles (BSA-NPs) are biocompatible and biodegradable carriers found across drug delivery, diagnostics, and biomedical studies [8]. BSA is a protein sourced from the blood of a cow and is popular due to its stability, lack of toxicity, and capacity for the binding of many drugs and bioactive compounds [9]. The nanoparticles (NPs) can be formulated employing techniques such as desolvation, emulsification, or thermal gelation, giving very good control of particle size and drug loading [10]. BSA-NPs may enhance the solubility, stability, and controlled release of drugs, allowing them to be used for targeted therapy in cancer and other diseases [11]. Compared to synthetic polymers such as poly{lactic-co-glycolic acid} (PLGA), BSA offers other advantages, such as avoidance of acidic degradation products, ease of scale-up, and the presence of functional groups that allow for site-specific modifications and targeted delivery.

Lenalidomide (LD) is an orally administered drug primarily used to treat various forms of blood cancers, including multiple myeloma and myelodysplastic syndromes [12]. It is commercially available in capsule form [13], with common side effects such as diarrhoea, nausea, and loss of appetite [14].

Several nanoformulations of LD have been explored in the literature, including LD cocrystals [15], mesoporous silica NPs for LD [16], and PLGA-based LD nanocarriers [17]. However, BSA-loaded LD formulations have not been reported. Taking into account BSA's superior biological properties and drug-binding ability, its application in LD delivery presents a novel strategy for enhancing therapeutic efficacy, solubility, and controlled release.

BSA-loaded nanocarriers have shown promising applications in cancer therapy, particularly in targeted drug delivery and tumor microenvironment modulation. Notable examples include Paclitaxel-loaded BSA-NPs [18], Doxorubicin-loaded BSA nanocarriers [19], and BSA@IR780-loaded mesoporous polydopamine NPs [20], all of which demonstrate enhanced therapeutic efficacy through improved bioavailability and selective tumor targeting.

In this study, LD was successfully incorporated into BSA-NPs, which were characterized based on particle size, zeta potential, and EE. BBD was used to optimize the LD-loaded BSA-NPs (LD-BSA-NPs). The optimized formulation was then evaluated for its cytotoxic potential against U266 cells, ensuring effective drug delivery and therapeutic performance.

MATERIALS AND METHODS

Materials

LD was purchased from MSN Labs. BSA, Ethanol, Glutaraldehyde, Methanol, dimethyl sulfoxide (DMSO**)**, distilled water, phosphate buffer saline (PBS), sodium hydroxide, and potassium dihydrogen phosphate were purchased from SD Fine Chemicals.

Preparation of LD-BSA-NPs

LD-BSA-NPs were prepared using the desolvation method [21], where BSA was first dissolved in distilled water at a controlled pH (pH-9) and stirred until fully solubilized. LD, typically pre-dissolved in a small amount of organic solvents like DMSO (10%-20%), was added to the BSA solution (10 ml) under continuous stirring. A desolvating agent such as ethanol (100 µl** per min) was then slowly introduced to induce the formation of NPs through protein precipitation. To stabilize these particles, a crosslinking agent like glutaraldehyde (58µl* of 8%) was added [22]. The resulting NPs were purified by centrifugation and washing to remove free drugs and residual chemicals, followed by lyophilization for storage. The final formulation was characterized by size, drug loading efficiency, surface charge, and drug release behavior, making it a promising delivery system for targeted cancer therapy.

Design of experiments (DoE)

A DoE approach was employed using the BBD to investigate the relationship between three independent variables-amount of BSA (X_1), quantity of DMSO (X_2), and stirring speed (X_3)-and their effects on particle size (Y_1), EE% (Y_2), and zeta potential (Y_3). Based on preliminary trials and literature evidence, X_1 was varied between 50 mg and 150 mg, X_2 between 10% v/v and 20% v/v, and X_3 was set within the range of 500 to 1000 rpm [23-25].

Table 1: Levels obtained from response surface model (RSM) design for independent variables

Independent variable (X)	Unit	Coded level		
		Low(-1)	Mid(0)	High(+1)
X1	mg	50	100	150
X2	% v/v	10	15	20
X3	rpm	500	750	1000
Dependent variable (Y) Requirement				
Y1	nm	minimize		
Y2	%	maximize		
Y3	mV	-25mV to-30mV		

Mili volt (mV), nano meter (nm)

Characterization of LD-BSA-NPs

Particle size and zeta potential

The prepared NPs were washed with double-distilled water, which was filtered through 0.22µm, several times before particle size analysis. The average particle size and zeta potential of the LD-BSA-NPs were determined by a particle size analyzer (Malvern Instruments Ltd, UK), which allows sample measurement in the range of 0.020-2000µm [26].

EE estimation

The previously described indirect method was used to calculate the EE% [27]. Using this procedure, the amount of free or unentrapped LD in the supernatant of each formulation following centrifugation at 12,000 rpm and 4 °C for 20 min using a cooling centrifuge (Remi, India) was assessed [28]. The amount of free LD was measured at 255 nm using a spectrophotometric technique (Spectro UV-VIS double beam, Lab India 3200). The EE% was calculated using the following equations:

$$EE\% = \frac{\text{Mass of drug in Nanoparticles}}{\text{Mass of the drug in Formulation}} \times 100$$

FTIR and DSC study

FTIR spectrophotometer (Perkin Elmer, USA) was employed to record the spectrum of each of the LD-BSA-NPs, and free LD. At 25 °C, the spectra were recorded in the 500–4000 cm−1 region (Berthomieu and Hienerwadel 2009). Furthermore, the thermograms of LD-BSA-NPs, pure LD, were estimated using a DSC analyser (PerkinElmer, USA). Each sample's dry powder (about 3 mg) was heated in a sealed aluminium pan at 10 °C per minute under nitrogen. A plain aluminum pan, as a reference, was used in all runs [29].

Morphological study by TEM

Using TEM (JEOL 100CX; JEOL Inc., Peabody, MA, USA) at an accelerating voltage of 80 kV, the morphology of the Opt-LD-BSA-NPs was examined. The Opt-LD-BSA-NPs formulation was diluted from 1 to 0.01% w/w and treated in an ultrasonic bath (Model 3510, Branson MS) in order to reduce particle aggregation on the copper grid. For TEM analysis, a single drop of the modified mixture was dried and put on a copper grid coated with carbon [30].

In vitro drug release study

The study used the dialysis bag technique to track drug-release patterns from LD-BSA-NPs. The release patterns were examined at a pH of 5.5 to mimic the acidic tumor microenvironment. The dialysis ag (12‑14kDa MWCO, Spectra/ProR4 Dialysis Membrane; Spectrum Laboratories, Inc., Rancho Dominguez, CA) was filled with 1 mg of the drug in its free form or a formulation volume equivalent to 1 mg of the drug. Dialysis bags were then submerged in 200 ml of acetate buffer, pH 5, containing TritonX-100 (1%), and kept in a shaking water bath (AZZOTA corporation, USA). Drug samples were withdrawn and analysed at 255 nm using a spectrophotometric technique (Spectro UV-VIS double beam, Lab India 3200) [31].

Cell line study

Human multiple myeloma U266 cells were acquired from the National Centre for Cellular Sciences (NCCS), Pune, India. The cells were 9ultured in minimal essential medium, supplemented with 10% fetal bovine serum (FBS), 3% L-glutamine, 100 U/ml penicillin-G, and 100 µg/ml streptomycin (Himedia), within a humidified atmosphere of 5% CO_2 and 95% air, maintained at 37±2 °C [32]. For cytotoxicity assays, 1 lakh cells per millilitre of the U266 cell suspension were seeded into a 96-well microtiter plate. After 24 h of incubation, a fresh medium containing varying concentrations of Opt-LD-BSA-NPs suspension was introduced. A working concentration of 10 mg/ml was prepared by dissolving 100.5 mg of NPs in 10.05 ml of PBS and subsequently filtering through a 0.22 µm filter before each assay. Blank control cells, which did not receive test samples, were incubated with PBS. The negligible presence of PBS in the wells was confirmed not to interfere with experimental outcomes.

Pharmacokinetic study

All the animal investigations were performed as per the requisite protocol approved by the institutional animal ethics committee (IAEC) of Chaitanya Deemed to be University, Hanamkonda, Telangana, with certificate no (005/2024/1963/PO/RC/S/17). *In vivo* studies were carried out in healthy male Wistar rats of 150-200g. The animals were housed in individual cages in the animal house for 10 days before the initiation of the study to facilitate environmental acclimatization and had access to feed and water *ad libitum*. 12-hour circadian rhythms were maintained, and the

temperature was kept constant throughout the study period. The animals were divided into two groups, each containing six animals. The animal dose (2.59 mg/kg) was chosen based on the surface area ratio from human to rat. Group 1 was treated with pure LD, and Group 2 was treated with Opt-LD-BSA-NPs. Blood samples, each not more than 500 µl**, were withdrawn from the tail vein at 0, 0.5, 1, 2, 3, 4, 6, 8, 10, 12, and 24 h intervals using a sterilized syringe. Fasting blood samples (0^{th} h) were withdrawn early in the morning. The blood samples were collected in radioimmunoassay (RIA)-vials containing anticoagulant (100 µl** of 11% sodium citrate) and centrifuged at 4000 rpm for 15 min to separate the plasma and stored at-20 °C. The plasma samples were deproteinized by mixing the samples with equal volumes of 10% perchloric acid and vortexing for 2 min, followed by centrifugation at 4000 rpm for 15 min [33]. The supernatant liquid was separated and analyzed. The amount of LD in plasma samples was estimated using high-performance liquid chromatography (HPLC) at optimized chromatographic conditions.

RESULTS AND DISCUSSION

Preparation and characterization of LD-BSA-NPs

Seventeen different batches of LD-BSA-NPs were prepared by the desolvation method. The Particle size was found in the range 110.9 nm to 182.8 nm. The EE% was in the range of 60.1-94.8%.

Optimization

The polynomial equation obtained indicates the effect of the interaction of dependent variables on independent variables. A positive value in the equation represents a promising effect, and a negative value represents a disapproving effect.

Particle size

The particle size of all 17 batches of LD-BSA-NP is given in table 2. As observed from table 2, particle size ranged from 110.9±13.02 nm to 182.8±10.33 nm. Further polynomial equations showed that the relation between particle size and the independent variables and their interactions significantly affected the particle size, as represented in table 3.

$$\text{Particle size } (Y_1) = 145.28+29.90X_1+0.6500X_2-3.30X_3+2.70X_1X_2+1.05X_1X_3-6.85X_2X_3-8.74X_1^2+11.91X_2^2+9.46X_3^2$$

The Quadratic model table (table 3) showed an F value of 36.31 and a P value of<0.0001, indicating a significant response. An increase in particle size with higher X_1 was observed from the quadratic equation. This is due to elevated BSA levels increasing the viscosity of the medium, which can slow down diffusion and promote the formation of larger particles due to reduced nucleation rates and enhanced growth phases. Similar results were reported by Tanjung YP *et al.* in 2024 [34]. The X_2 affects the particle size. This is because a higher DMSO content may lead to slower desolvation, promoting the formation of larger particles due to extended growth phases [35]. At lower rotation speeds, an increased particle size was observed, and as the speed increased, the particle size was found to reduce. This is because increased shear force promotes better dispersion of the desolvated protein droplets, preventing coalescence and leading to more uniform and smaller NPs [36] (fig. 1).

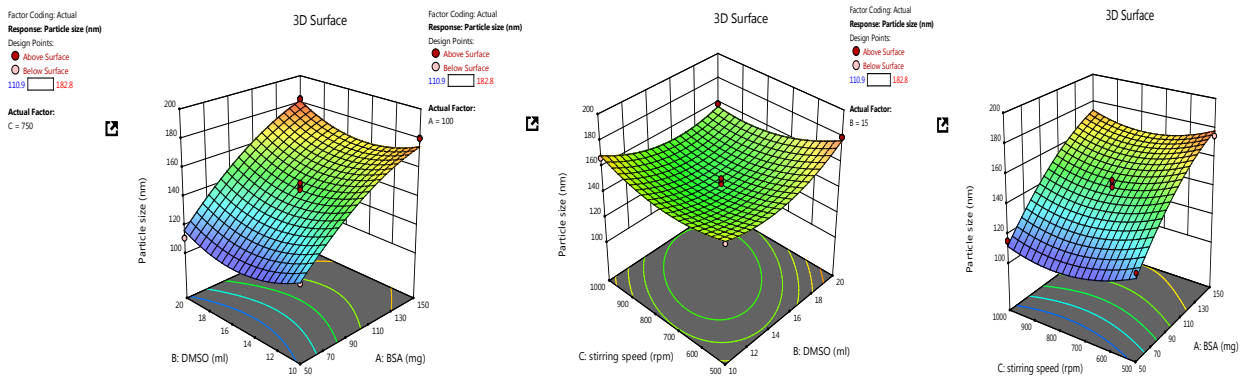

Fig. 1: Effect of the independent variable on particle size

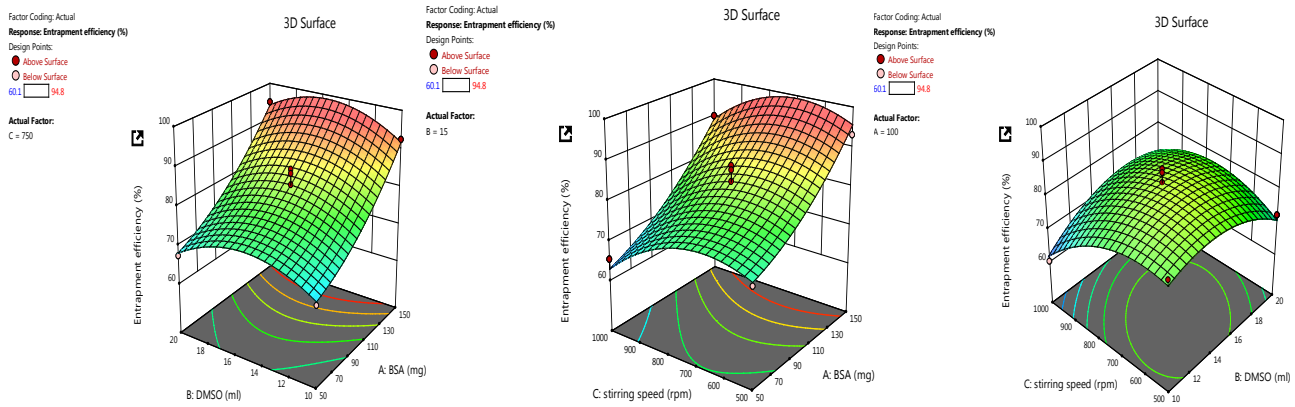

Fig. 2: Effect of independent variable on EE

EE analysis

The EE% for 17 formulations was found to be from 60.1±9.01% to 94.80±9.14% (table 2). A major goal of the current study is to maximize the entrapment of the drug into the NPs to increase the drug concentration at the site of action. The quadratic equation for EE% is

$$EE(Y2)=83.04+12.40X_1+0.5375X_2-3.94X_3+0.5500X_1X_2+0.7000X_1X_3+4.32X_2X_3+3.42X_1^2-6.01X_2^2-6.51X_3^2$$

The Quadratic model table for EE% (table 3) showed an F value of 17.81 and a P value of<0.005, indicating a significant response. The EE was found to increase by increasing X_1, as observed in the quadratic equation. The increase in the EE% at a higher albumin amount is due to the higher availability of the albumin surrounding the drug [37]. As the albumin concentration increases, more NPs would be formed, which in turn increases the chance for better drug encapsulation. The DMSO concentration effect on EE. DMSO improves the solubility of hydrophobic drugs like LD, allowing better dispersion in the aqueous BSA solution. This facilitates stronger drug-protein interactions during NP formation, potentially increasing EE% [38] (fig. 2).

Table 2: BBD for LD-BSA-NP with responses

Formulation	X_1	X_2	X_3	Particle size	EE%	Zeta potential
LD-BSA-NP1	100	15	750	143.4±12.30	78.8±7.23	-27.9±0.07
LD-BSA-NP2	100	15	750	140.2±10.01	80.2±8.04	-25.4±0.13
LD-BSA-NP3	100	15	750	147.3±11.26	83.1±9.11	-29.7±0.11
LD-BSA-NP4	100	20	500	179.8±11.44	72.3±7.03	-20 ±0.18
LD-BSA-NP5	50	20	750	110.9±13.02	67.3±8.55	-17.1±0.14
LD-BSA-NP6	100	15	750	150.1±12.11	87.1±9.24	-29.7±0.12
LD-BSA-NP7	50	10	750	119.5±10.46	67.2±6.25	-26.4±0.16
LD-BSA-NP8	150	15	1000	170.4±10.31	90 ±9.11	-24.4±0.15
LD-BSA-NP9	100	10	500	160.3±12.44	80 ±7.35	-30 ±0.08
LD-BSA-NP10	150	10	750	180.6±13.11	92.5±8.07	-20.6±0.44
LD-BSA-NP11	150	20	750	182.8±10.33	94.8±9.14	-15.3±0.21
LD-BSA-NP12	50	15	1000	115.2±11.21	65.4±7.47	-32.8±0.19
LD-BSA-NP13	100	20	1000	159.3±12.26	69.7±7.32	-22.3±0.08
LD-BSA-NP14	150	15	500	174.7±13.26	93.1±8.36	-25.2±0.13
LD-BSA-NP15	50	15	500	123.7±10.06	71.3±7.11	-31.6±0.14
LD-BSA-NP16	100	10	1000	167.2±12.31	60.1±9.01	-28.1±0.12
LD-BSA-NP17	100	15	750	145.4±10.31	86±8.59	-28.2±0.18

(n=3, mean ±SD)

Zeta potential

Zeta potential plays a critical role in determining the stability of NPs. The zeta potential was obtained in a range from-15.3±0.21mV to-29.7 ±0.12mV (table 2). The quadratic equation for zeta potential is as follows

$$\text{Zeta potential } (Y_3)=26.86+2.80X_1+3.80X_2-0.1000X_3-1.0000X_1X_2+0.5000X_1X_3-1.05X_2X_3+1.80X_1^2+5.21X_2^2-3.44X_3^2$$

The Quadratic model table for zeta potential (table 3) showed an F value of 8.26 and a P value of<0.0055, indicating a significant response. An increase in the concentration of BSA increases the zeta potential, which is because higher BSA concentration tends to increase the availability of surface amino and carboxyl groups, which can lead to more negative or positive zeta potential, depending on the pH of the medium [39] (fig. 3).

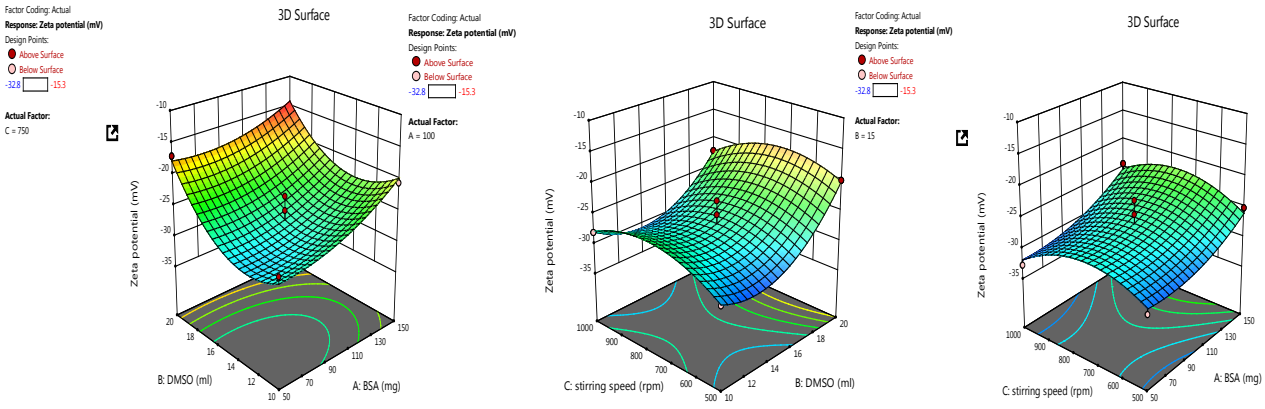

Fig. 3: Effect of the independent variable on zeta potential

Table 3: BBD regression coefficients with p-values and quadratic equation

Parameter	Responses					
	Particle size		EE%		Zeta potential	
	F-value	p-value	F-value	p-value	F-value	p-value
Model	36.31	<0.0001	17.81	0.0005	8.26	0.0055
Lack of fit	3.07	0.1536	0.7261	0.5873	0.3263	0.8077
R^2	0.9790	0.9582	0.9139			
Adjusted R^2	0.9521	0.9044	0.8032			
Predicted R^2	0.7562	0.7217	0.6211			
Suggested model quadratic						
$Y_1=+145.28+29.90X_1+0.6500X_2-3.30X_3+2.70X_1X_2+1.05X_1X_3-6.85X_2X_3-8.74X_1^2+11.91X_2^2+9.46X_3^2$						
$Y_2=+83.04+12.40X_1+0.5375X_2-3.94X_3+0.5500X_1X_2+0.7000X_1X_3+4.32X_2X_3+3.42X_1^2-6.01X_2^2-6.51X_3^2$						
$Y_3=-26.86+2.80X_1+3.80X_2-0.1000X_3-1.0000X_1X_2+0.5000X_1X_3-1.05X_2X_3+1.80X_1^2+5.21X_2^2-3.44X_3^2$						

Data optimization and model validation for opt-LD-BSA-NPs

The optimized Opt-LD-BSA-NPs formulation was selected by applying constraints on the dependent factors, as shown in table 4. Point prediction of the DoE software 12 was used to determine the optimized NPs based on closeness of desirability factor close to 1, which predicted the optimized process parameters to be X_1 as 100 mg, X_2 as 15 ml, X_3 as 750 rpm with predicted values of responses Y_1 as 145.28 nm, Y_2 as 86.04% and Y_2 as 26.86mV. The Opt-LD-BSA-NPs was developed and characterized for particle size, EE% and zeta potential. The experimental value for responses Y_1 as 147 nm, Y_2 as 85%, and Y_3 as 28.01mV of optimized formulation was found in good agreement with the predicted values generated by the RSM and the result assures the validity of RSM.

Table 4: Predicted and observed responses for optimized formulation

Responses	Predicted	Observed	% of Error
Particle size(nm)	145.28	147	1.18
EE %	83.04	85	2.30
Zeta potential(mV)	-26.86	-28.01	4.1

Characterization study on the optimized formulation

TEM analysis

The morphological analysis of albumin NPs in fig. 4a shows spherical particles of about, with a uniform particle size distribution, which coincides with the diffractive light scattering (DLS) measurements. The observed polydispersity index (PDI) of 0.145 and particle size range of 110–183 nm in the BSA-NP formulation suggest moderate monodispersity, which likely results from controlled desolvation kinetics, stabilizing intermolecular interactions among albumin molecules, and effective crosslinking-ensuring a narrowly distributed particle population with minimal aggregation [40].

Zeta potential and PDI

Zeta potential indicates the stability of the NPs in the dispersion through electrostatic repulsion between the particles. As the value increases, it gives an indication of more repulsion between the NPs, reducing the tendency of aggregation that could occur between the NPs. The zeta potential for the Opt-LD-BSA-NPs was found to be–28.01 mV. The negative charge might be due to the preparation of the albumin at a pH higher than the isoelectric point of the protein, leading to the ionization of the carboxyl-terminal of the protein, and hence imparting a negative charge. The PDI was found to be 0.145, which indicates the homogeneity of the distribution within the formed NPs.

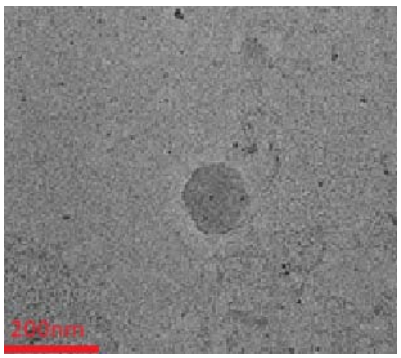

Fig. 4a: TEM Image

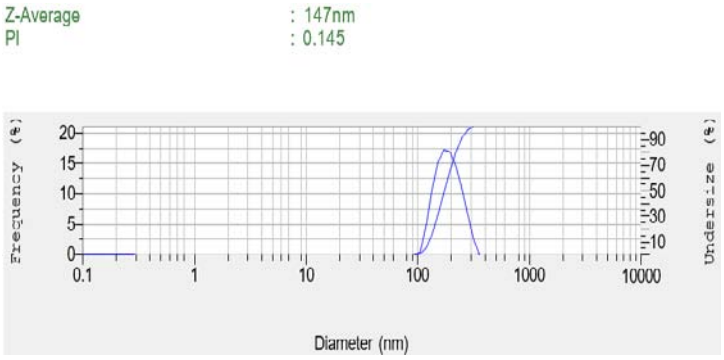

Fig. 4b: Particle size distribution

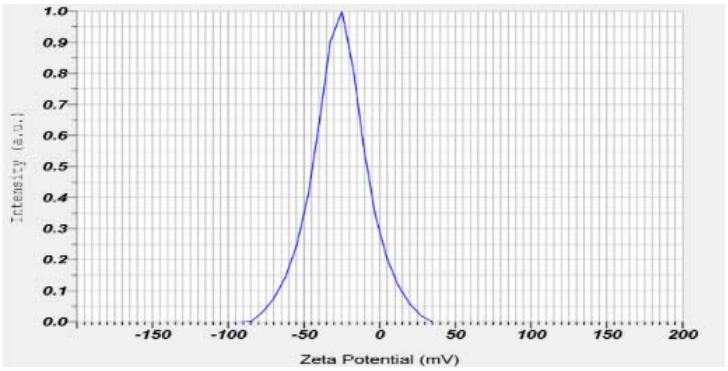

Fig. 4c: Zeta potential

In vitro drug release

The release of LD from both the pure LD suspension and the Opt-LD-BSA-NPs is shown in fig. 5. The release of LD from BSA-NPs showed a biphasic release, with an initial burst effect, which is followed by a sustained release over 24 h. A sudden burst release of about 55.68% was observed within 4 h from Opt-LD-BSA-NPs, followed by a slower release over 24 h, whereas the pure LD suspension was completely released (99.32%) within 4 h. The initial burst effect might be due to the free unencapsulated drug and the drug on the surface of the NPs. The sustained release pattern may be attributed to the drug incorporated in the core of the NPs' matrix. It should be mentioned that the sustained release effect is in great favor for cancer targeting, as it is required for the anticancer drugs to have a slow release in the blood to reduce their side effects on the normal cells, whereas when it reaches the cancer cells, it should be high.

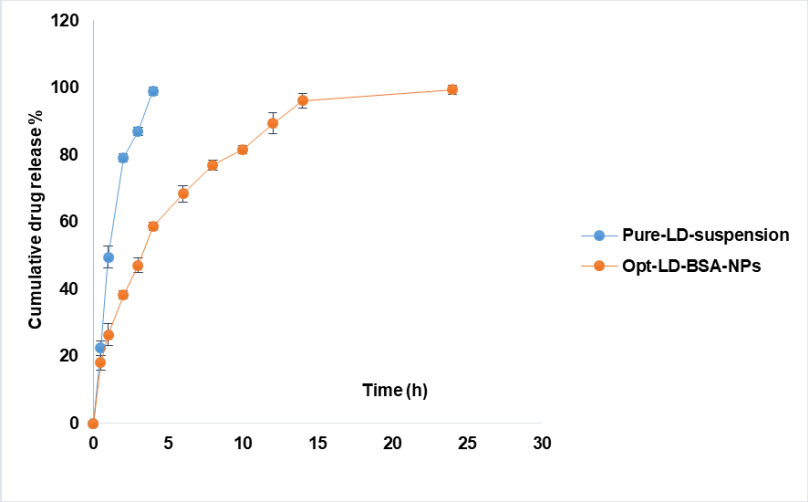

Fig. 5: Drug release study

DSC and FTIR studies of Opt-LD-BSA-NPs

The DSC thermograms of pure LD and Opt-LD-BSA-NPs are shown in fig. 6. The DSC curve of LD exhibits an exothermic peak at a peak temperature of 270 °C, corresponding to its melting point. As per the DSC graph of Opt-LD-BSA-NPs, the characteristic exothermic peak of LD was observed with minimal intensity and shifted to a lower temperature range. This indicates the conversion of the crystalline nature of LD to an amorphous form, which ensures better stability. Furthermore, it also confirms that LD was entrapped in BSA-NPs. Reported findings have suggested that with an increase in the amorphous nature of the therapeutic system, a corresponding increase in the efficiency of delivery is observed by Abdelwahed *et al.* in 2006.

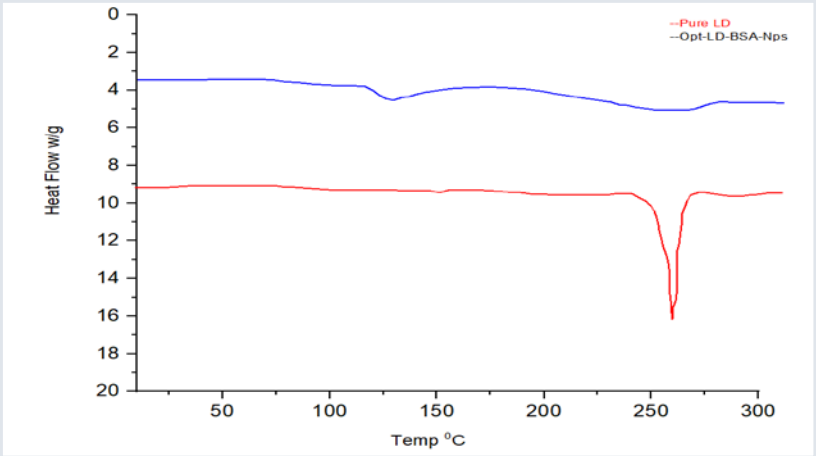

Fig. 6: DSC study

The FTIR of pure LD and Opt-LD-BSA-NPs are described in fig. 7. The Pure LD FTIR spectrum reveals key functional groups, with amide absorption around 1600–1700 cm^{-1}, aromatic ring peaks near 1500 cm^{-1} and 3000 cm^{-1}, and broad-NH/-OH bands in the 3200–3500 cm^{-1} range the FTIR spectrum of the Opt-LD-BSA-NPs revealed distinct shifts in the amide bands, confirming successful drug encapsulation and stable protein interactions.

Cytotoxicity studies

The effects of pure LD and Opt-LD-BSA-NPs on the extent of cell viability of U266 cells for 72 h were examined by 3-(4,5-di methyl thiazol-2-yl)-2,5-diphenyl tetrazolium bromide (MTT) assay. Seven concentrations (1-100 µg/ml) of pure LD and Opt-LD-BSA-NPs were prepared and tested, yielding proof that the NPs exhibited significant toxicity against U266 cells as compared to pure LD (fig. 8). The cytotoxic concentration at which 50% of the cells die (CTC50) value for NPs was calculated from the concentration and subsequent response. It was found that at a 100µg/ml concentration, Opt-LD-BSA-NPs are highly cytotoxic compared to pure LD. The IC50 value for pure LD was found to be 49.42%, whereas the Opt-LD-BSA-NPs exhibited a significantly lower IC50 of 29.70%, indicating enhanced cytotoxic efficacy. This reduction suggests that NP encapsulation improves drug delivery, likely due to better cellular uptake, sustained release, and increased bioavailability of LD at the target site.

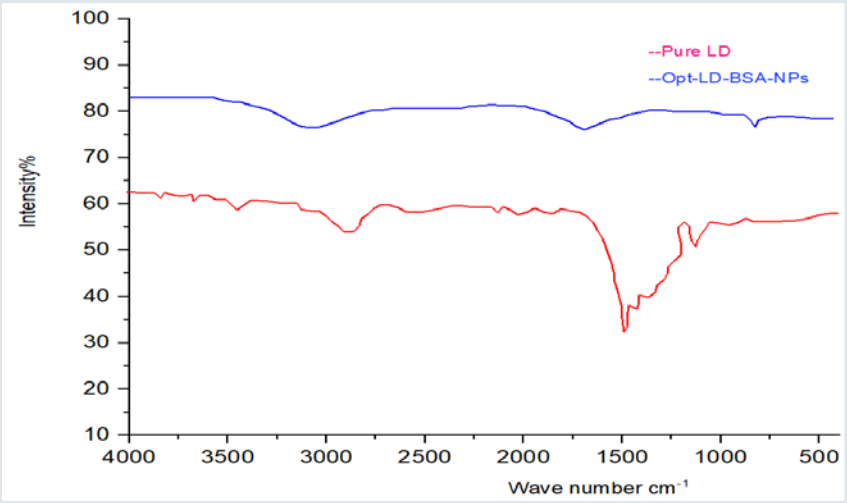

Fig. 7: FTIR study

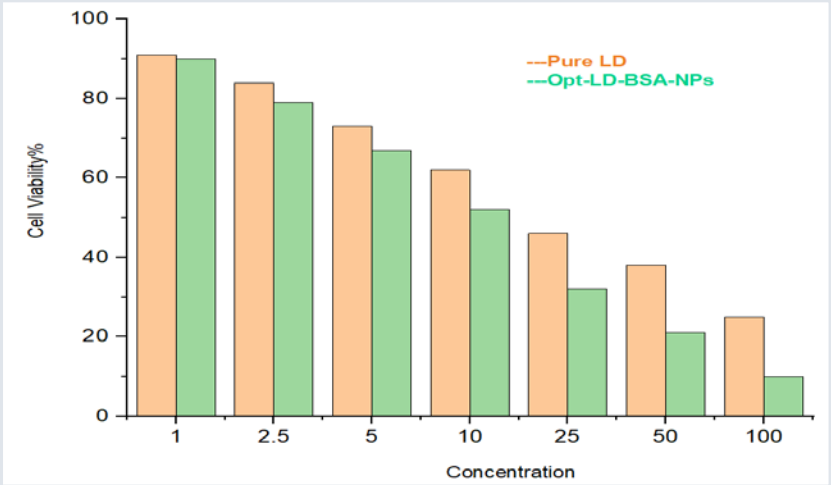

Fig. 8: Cytotoxic study

***In vivo* pharmacokinetic studies**

The formulations (LD aqueous suspension, dispersion of the Opt-LD-BSA-NPs) were administered by oral gavage with a single dose of 30 mg/kg. The NPs were dispersed in ultra-pure water. Table 5 and fig. 9 show the pharmacokinetic data of the drug suspension and NPs. Fig. 9 depicts a remarkable difference in bioavailability between Opt-LD-BSA-NPs and pure LD suspension. After oral administration of pure LD suspension, the drug was rapidly absorbed, and a C_{max} of 0.98 µg/ml was reached in 1.5 h. Consequently, the plasma concentration decreased abruptly, as the drug was rapidly distributed and metabolized and was detected up to 24 h after administration, resulting in low AUC (6.3025 h. µg/ml), area under 1st movement curve (AUMC) (31.775h^2. µg/ml), and low $t_{½}$ (4 h). The mean residence time (MRT) for Pure LD was found to be 5.041. Fig. 9 shows the peak plasma concentration (C_{max}) for Opt-LD-BSA-NPs of approximately 2.5 µg/ml.

Table 5: Pharmacokinetic parameters of LD after oral administration of pure LD suspension and Opt-LD-BSA-NPs dispersion at the dose of 30 mg/kg

Parameter	Pure LD Suspension	Opt-LD-BSA-NPs
C_{max} (µg/ml)	0.98±	2.5
AUC (µg. h/ml)	6.3025	22.47
AUMC(µg/ml. h^2)	31.775	182.13
K_e(h^{-1})	0.173	0.05775
$t_{1/2}$(h)	4	12
MRT	5.041	8.105

Similarly, table 5 depicts the pharmacokinetic parameters C_{max}, AUC, AUMC, and MRT of Opt-LD-BSA-NPs. From table 5, it can be perceived that the C_{max} value for Opt-LD-BSA-NPs (2.5 µg/ml) was significantly higher than that of the LD suspension (0.98 µg/ml). In the same way, the $t_{½}$ was rapid for Opt-LD-BSA-NPs (12 h), when compared to pure LD suspension (4 h). The AUC for Opt-LD-BSA-NPs is 22.47 µg/ml. h, which is 3 times more than the pure LD suspension (6.3025µg/ml. h).

This may be due to the primarily related prolonged absorption phase and sustained release of LD from BSA-NPs. Likewise, the MRT

for Opt-LD-BSA-NPs is 8.105s, which is almost 1.6 times more than the pure LD-suspension. Overall, our results suggest that Opt-LD-BSA-NPs are most likely to have great potential as a therapeutic, with enhanced pharmacokinetic profiles [41].

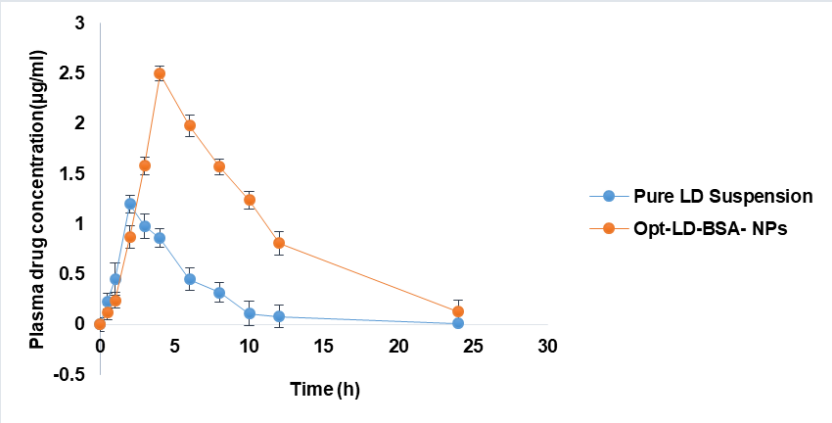

Fig. 9: Plasma concentration time profiles of LD in Wistar rats: (a) Pure LD suspension, (b) Opt-LD-BSA-NPs

CONCLUSION

NPs of a poorly soluble drug, LD, were successfully formulated by the nano-precipitation method using BSA as a polymer. The particle size, zeta potential, and TEM reports confirmed that the size of Opt-LD-BSA-NPs was below 200 nm with a spherical shape and uniform size distribution. DSC and FTIR analysis of NPs confirmed the conversion of the crystalline nature of LD to an amorphous form and drug entrapment within the NPs. Cytotoxic studies suggested that Opt-LD-BSA-NPs were toxic to U266 cancer cells. *In vitro* and *in vivo* studies confirmed that LD-BSA-NPs exhibit increased bioavailability with sustained release up to 24 h. Due to their hydrophobic nature, conventional chemotherapeutics of LD suffer from poor solubility and an inability to penetrate the tumors (poor bioavailability). This results in grave side effects that include immune system depletion and metastasis to neighbouring organs. Hence, the present BSA-NPs can effectively solve the solubility problem and enhance the bioavailability of LD.

FUNDING

Nil

AUTHORS CONTRIBUTIONS

Sameena Begum: Conceptualization, investigation, data curation, writing original draft, Niranjan Panda: Writing, review, and editing Ch. Praveena: Supervision

CONFLICT OF INTERESTS

Declared none

REFERENCES

1. Al Ostoot FH, Salah S, Khanum SA. An overview of cancer biology, pathophysiological development and it's treatment modalities: current challenges of cancer anti-angiogenic therapy. Cancer Investig. 2024 Aug 8;42(7):559-604. doi: 10.1080/07357907.2024.2361295, PMID 38874308.
2. Sriharikrishnaa S, Suresh PS, Prasada S. An introduction to fundamentals of cancer biology. In: Mazumder N, Kistenev YV, Borisova E, Prasada KS, editors. Optical polarimetric modalities for biomedical research. Berlin: Springer International Publishing; 2023 Jul 23. p. 307-30. doi: 10.1007/978-3-031-31852-8_11.
3. Sobti RC, Gosipatala SB, Sharma M, Reddy P, Khalko RK, Kaur T. Types of cancers, epidemiology and molecular insights. In: Sobti RC, Ganguly NK, Kumar R, editors. Handbook of Oncobiology: from Basic to Clinical Sciences. Singapore: Springer Nature; 2023 Oct 10. p. 1-36. doi: 10.1007/978-981-99-2196-6_1-1.
4. Ahmad I, Jasim SA, Sharma MK, S RJ, Hjazi A, Mohammed JS. New paradigms to break barriers in early cancer detection for improved prognosis and treatment outcomes. J Gene Med. 2024 Aug;26(8):e3730. doi: 10.1002/jgm.3730, PMID 39152771.
5. Ahmed MB, Alghamdi AA, Islam SU, Ahsan H, Lee YS. The complex roles of DNA repair pathways inhibitors, hyperthermia and contact inhibition in cell cycle halts. Mini Rev Med Chem. 2023 Mar 1;23(5):514-29. doi: 10.2174/1389557522666220826141837, PMID 36029081.
6. Mazingi D, Lakhoo K. Cancer development and progression and the hallmarks of cancer. In: Lakhoo K, Abdelhafeez AH, Abib S, editors. Pediatric surgical oncology. Berlin: Springer International Publishing; 2023 Jun 14. p. 1-15. doi: 10.1007/978-3-030-71113-9_23-1.
7. Wang H, Guo M, Wei H, Chen Y. Targeting p53 pathways: mechanisms, structures and advances in therapy. Signal Transduct Target Ther. 2023 Mar 1;8(1):92. doi: 10.1038/s41392-023-01347-1, PMID 36859359.
8. Wang Y, Iqbal H, Ur Rehman U, Zhai L, Yuan Z, Razzaq A. Albumin-based nanodevices for breast cancer diagnosis and therapy. J Drug Deliv Sci Technol. 2023 Jan 1;79:104072. doi: 10.1016/j.jddst.2022.104072.
9. Behera S, Mohanty P, Dash PP, Mohapatra P, Shubhadarshinee L, Behura R. Selective binding of bovine serum albumin (BSA): a comprehensive review. Biointerface Res Appl Chem. 2023;13(6):555. doi: 10.33263/BRIAC136.555.
10. Mardikasari SA, Katona G, Csoka I. Serum albumin in nasal drug delivery systems: exploring the role and application. Pharmaceutics. 2024 Oct 11;16(10):1322. doi: 10.3390/pharmaceutics16101322, PMID 39458651.
11. Lawal RA, Banjoko O, Ndulue C, Adebeshin ST, Sharif A, Ighodaro OE. Improved side effect profile of alternate-day dosing of lenalidomide. Cureus. 2024 Mar 1;16(3):e55317. doi: 10.7759/cureus.55317, PMID 38559519.
12. Banchi M, Cox MC, Bocci G. Metronomic chemotherapy in hematology: lessons from preclinical and clinical studies to build a solid rationale for future schedules. Cancer Lett. 2024 Jun 1;591:216900. doi: 10.1016/j.canlet.2024.216900, PMID 38636896.
13. Takahashi Y, Nagamine A, Kaneta A, Yashima H, Obayashi K, Araki T. Risk of exposure of patients family members to lenalidomide at home. Eur J Hosp Pharm. 2024 Nov 1;31(6):555-9. doi: 10.1136/ejhpharm-2022-003632, PMID 37339864.
14. Nadeem O, Ailawadhi S, Khouri J, Williams L, Catamero D, Maples K. Management of adverse events associated with pomalidomide-based combinations in patients with relapsed/refractory multiple myeloma. Cancers. 2024 Feb 29;16(5):1023. doi: 10.3390/cancers16051023, PMID 38473381.
15. Screen MA, Tomkinson G, McCabe JF, Askin S, Mahon CS, Wilson MR. Designing lenalidomide cocrystals with an extended release profile for improved pulmonary drug delivery. New J Chem. 2025;49(16):6535-43. doi: 10.1039/D5NJ00425J.

16. Gupta A, Moorkoth S, Moorkoth S, Dhas N. Central composite design aided optimization and validation of developed an eco-friendly HPLC method for the quantification of lenalidomide loaded mesoporous silica nanoparticles. J Appl Pharm Sci. 2024 Nov 25;15(1):89-101. doi: 10.7324/JAPS.2024.189998.
17. Aghaei Delche N, Kheiri R, Ghorbani Nejad B, Sheikhi M, Razavi MS, Rahimzadegan M. Recent progress in the intranasal PLGA-based drug delivery for neurodegenerative diseases treatment. Iran J Basic Med Sci. 2023;26(10):1107-19. doi: 10.22038/IJBMS.2023.70192.15264, PMID 37736505.
18. Kono Y, Sugaya T, Yasudome H, Ogiso H, Ogawara KI. Preparation of stable and monodisperse paclitaxel-loaded bovine serum albumin nanoparticles via intermolecular disulfide crosslinking. Biochem Biophys Rep. 2024 Jul 1;38:101713. doi: 10.1016/j.bbrep.2024.101713, PMID 38681670.
19. Hsu WH, Ku CL, Lai YR, Wang SS, Chou SH, Lin TH. Developing targeted drug delivery carriers for breast cancer using glutathione-sensitive doxorubicin-coupled glycated bovine serum albumin nanoparticles. Int J Biol Macromol. 2023 Sep 30;249:126114. doi: 10.1016/j.ijbiomac.2023.126114, PMID 37541475.
20. Yang S, Diao Y, Hang L, Qu H, Fang L, Guo W. BSA@IR780-loaded mesoporous polydopamine nanoparticles with enhanced photostability for multimodal imaging and photothermal therapy of tumors. Nanoscale Adv. 2025;7(8):2182-94. doi: 10.1039/D5NA00008D, PMID 40007568.
21. Hasan HJ, Ghareeb MM. Optimizing desolvation conditions for glutathione-cross-linked bovine serum albumin nanoparticles: implication for intravenous drug delivery. Cureus. 2024 Sep 16;16(9):e69514. doi: 10.7759/cureus.69514, PMID 39416524.
22. Behram T, Pervez S, Nawaz MA, Ahmad S, Jan AU, Rehman HU. Development of pectinase-based nanocatalyst by immobilization of pectinase on magnetic iron oxide nanoparticles using glutaraldehyde as crosslinking agent. Molecules. 2023 Jan 3;28(1):404. doi: 10.3390/molecules28010404, PMID 36615596.
23. Maiti R, Panigrahi S, Yin T, Huo M. Bovine serum albumin nanoparticles: constructing procedures on anticancer activities. Int J Adv Res Biol Sci. 2018;5(4):226-39. doi: 10.22192/ijarbs.
24. Jena S, Aksan A. Effect of high DMSO concentration on albumin during freezing and vitrification. RSC Adv. 2017;7(69):43611-20. doi: 10.1039/C7RA07556A.
25. Jahanshahi M, Najafpour G, Rahimnejad M. Applying the Taguchi method for optimized fabrication of bovine serum albumin (BSA) nanoparticles as drug delivery vehicles. Afr J Biotechnol. 2008;7(4):362-7. doi: 10.5897/AJB07.843.
26. Karri VV, Dhandapani NV, Mannemala SS, Radhakrishna K, Mulukutla S, Sudunagunta D. Ameliorating the antitumor activity of lenalidomide using PLGA nanoparticles for the treatment of multiple myeloma. Braz J Pharm Sci. 2017 Jun 22;53(2):e15185. doi: 10.1590/s2175-97902017000215185.
27. Panda N, Charan Panda K, Reddy AV, Reddy GV. Process optimization formulation and evaluation of hydrogel {guar gum-g-poly (acrylamide)} based doxofylline microbeads. Asian J Pharm Clin Res. 2014 Jul 1;7(3):60-5.
28. Mansour A, Fytory M, Ahmed OM, Rahman FE, El Sherbiny IM. *In vitro* and *in vivo* assessment of pH-responsive core-shell nanocarrier system for sequential delivery of methotrexate and 5-fluorouracil for the treatment of breast cancer. Int J Pharm. 2023 Dec 15;648:123608. doi: 10.1016/j.ijpharm.2023.123608, PMID 37972670.
29. Niranjan P, Reddy AV, Reddy GV, Panda KC. Formulation design and *in vitro* evaluation of zolmitriptan immediate release tablets using primojel and Ac-di-Sol. J Pharm Sci Res. 2015;7(8):545-53.
30. Sharma V, Sundaramurthy A. Surface modification of bare copper grids with charged polymers: a simple alternative for carbon-coated copper grids in transmission electron microscopy. Mater Lett. 2022 Feb 1;308:131204. doi: 10.1016/j.matlet.2021.131204.
31. Silva F, Sitia L, Allevi R, Bonizzi A, Sevieri M, Morasso C. Combined method to remove endotoxins from protein nanocages for drug delivery applications: the case of human ferritin. Pharmaceutics. 2021 Feb 6;13(2):229. doi: 10.3390/pharmaceutics13020229, PMID 33562060.
32. Terzi H, Altun A, Sencan M. *In vitro* comparison of the cytotoxic effects of statins on U266 myeloma cell line. Indian J Med Res. 2019 Dec 1;150(6):630-4. doi: 10.4103/ijmr.IJMR_672_18, PMID 32048627.
33. Panda N, Reddy AV, Reddy GV, Panda KC. Effect of different grades of HPMC and eudragit on drug release profile of doxofylline sustained release matrix tablets and *IVIVC* studies. Int Res J Pharm. 2015;6(8):493-504. doi: 10.7897/2230-8407.068100.
34. Tanjung YP, Dewi MK, Gatera VA, Barliana MI, Joni IM, Chaerunisaa AY. Factors affecting the synthesis of bovine serum albumin nanoparticles using the desolvation method. Nanotechnol Sci Appl. 2024 Dec 31;17:21-40. doi: 10.2147/NSA.S441324, PMID 38314401.
35. Wallerstein J, Akke M. Minute additions of DMSO affect protein dynamics measurements by NMR relaxation experiments through significant changes in solvent viscosity. ChemPhysChem. 2019 Jan 21;20(2):326-32. doi: 10.1002/cphc.201800626, PMID 30102005.
36. Magalhaes IS, Maurilio KB, De Souza DA, Tribst AA, Leite Junior BR. Application of roasting ultrasound and high-shear dispersion in pea protein extraction: yield parameters, macrostructural characteristics and technical functional properties. Food Bioprocess Technol. 2025 Apr 21;18(7):6550-63. doi: 10.1007/s11947-025-03852-3.
37. Spada A, Emami J, Tuszynski JA, Lavasanifar A. The uniqueness of albumin as a carrier in nanodrug delivery. Mol Pharm. 2021 Mar 31;18(5):1862-94. doi: 10.1021/acs.molpharmaceut.1c00046, PMID 33787270.
38. Shalmani AA, Wang A, Ahmed Z, Sheybanifard M, Mihyar R, Buhl EM. Tunable polymeric micelles for taxane and corticosteroid co-delivery. Drug Deliv Transl Res. 2024 Oct;14(10):2642-54. doi: 10.1007/s13346-023-01465-x, PMID 37962836.
39. Zaibudeen AW, Philip J. Adsorption of bovine serum albumin at oil-water interface in the presence of polyelectrolytes and nature of interaction forces. Colloids Surf A Physicochem Eng Aspects. 2019 Apr 5;566:38-47. doi: 10.1016/j.colsurfa.2019.01.014.
40. Wilson BK, Prudhomme RK. Nanoparticle size distribution quantification from transmission electron microscopy (TEM) of ruthenium tetroxide-stained polymeric nanoparticles. J Colloid Interface Sci. 2021 Dec 15;604:208-20. doi: 10.1016/j.jcis.2021.04.081, PMID 34265681.
41. Virani HA, Upadhyay MS, Pargi PM, Ashish P, Anovadiya. Evaluation of hypolipidemic activity of Opuntia elatior fruit juice in high-fat diet-induced hyperlipidemia in Wistar albino rats. Asian Journal of Pharmaceutical and Clinical Research. 2025;18(7):240-4. doi: 10.22159/ajpcr.2025v18i7.54619.